On the precision of neural computation with interaural time differences in the medial superior olive

Petr Marsalek[a,b,c] and Zbynek Bures[d,e]

[a]Institute of Pathological Physiology, First Medical Faculty, Charles University in Prague, U Nemocnice 5/478, 128 53, Praha 2, Czech Republic
[b]Department of Radioelectronics, Faculty of Electrical Engineering, Czech Technical University in Prague, Technická 2/1902, 166 27, Praha 6, Czech Republic
[d]Czech Institute of Informatics, Robotics and Cybernetics, Czech Technical University in Prague, Jugoslávských partyzánů 4/1903, 166 36, Praha 6, Czech Republic
[e]College of Polytechnics, Tolstého 16/1556, 586 01, Jihlava, Czech Republic
[c]Corresponding author: Petr.Marsalek@LF1.CUni.CZ

November 23, 2019

Abstract

We study a model of mammalian sound source localization in horizontal plane. Experiments on small rodents indicate that some mammals use broadly tuned channels of main left and right azimuth directions to perform the localization task. In human this neural computation is implemented by medial superior olive for low frequency sounds up to 1500 Hz. The description of the neural circuit implies existence of following parameters. Spike timing jitter, coincidence detection window length, sound frequency, among other input parameters, influence the output precision, measured by the just noticeable difference in direction signaled by the circuit. We use stochastic model with spiking neurons. We construct analytical formulas to estimate results of all numerical computations used in the model. We explore variations of the parameters mentioned above. Predictions of this model have straightforward applications in testing and designing stimulation protocols used in hearing aids and cochlear implants.

Keywords

binaural hearing, cochlear implant, coincidence detection, ergodic hypothesis, hearing aid, ideal observer, interaural time difference, just noticeable difference, lateral and medial superior olive, neuronal arithmetic, psychophysics, sound localization.

Abbreviations and symbols

f_{S}, sound frequency; F_{C}, critical sound frequency value; φ, sound phase; ILD, interaural level difference; IPD, interaural phase difference; ISI, inter-spike interval; ITD, interaural time difference; JND, just noticeable difference, also difference limen, or threshold; $K(.)$, K_{C}, K_S, K_X; A, B, C, ... proportionality constants; l, sound level, or rate of point process; LSO, lateral superior olive; MSO, medial superior olive; $R(.)$, R_{VS}, VS, vector strength; R_F, firing rate; σ, standard deviation; t_{J} timing jitter; t, Δt, time, time difference; T, T_{S}, T_{X}, sound periods, time constants.

1 Introduction

Mammalian sound localization circuits contain two nuclei in the auditory brainstem, the medial and the lateral superior olive, MSO and LSO. Neurons in these nuclei are the first binaural neurons in the auditory pathway, they are connected to both ears.

This article presents description of information encoding and neural computation in the MSO obtained mostly with analytical computations. Using the analytical tools we extend quantitative results obtained by numerical computations in [Sanda and Marsalek, 2012]. We compare this analytical MSO description to the LSO description in [Bures and Marsalek, 2013] to arrive to unified description of neural circuits in the superior olive. We use this description to find maximum spike timing precision attained by the following two modalities, natural and electrical hearing. Apparently, low and high frequency sound localization use different neuronal mechanism, because low and high sound frequencies are encoded by distinctive codes. In a simplified view, low frequencies are encoded by both spike timing and tonotopic organization, and high frequencies are encoded solely by the tonotopic organization.

Due to the physical nature of the binaural sound, the MSO neurons process spike timing differences, Interaural Time Differences, ITDs, in the range of tens of microseconds, 10 μs. The MSO processes low frequency sounds, in human this is from 20 Hz to not more than 2 kHz. The LSO processes high frequency sounds, in human this is from 1 kHz up to 20 kHz, with the use of Interaural Level Differences, ILDs. The overlapping region is known to have a sensitivity drop at 1.5 kHz [Mills, 1958].

Firing rate, first spike latency and individual spike timings are used in neural system coding, especially in the auditory pathway. The highest known spike timing precision that has been proven to be utilized in the mammalian auditory system is the motor response in a bat. In behavioral experiment, the big brown bat, *Eptesicus fuscus* catches tidbit larvae of the meal-worm beetle *Tenebrio molitor*. The motor precision is in the range of hundreds of nanoseconds, 100 ns, and auditory separation of ultrasound echoes in the bats sonar sense is in the order of microsecond units, 1 μs [Simmons et al., 1998]. Comparable performance of the human MSO is in the range of microseconds, 10 μs and is reported to be improved two- to five-fold after several hours of training.

Different neural mechanisms are employed in the two nuclei. It has been reported that computation in the MSO is independent on sound intensity [Grothe et al., 2010]. With higher sound intensity, first spike latency is shortening. Relation of this dependence to ITD and ILD has been described, yet it is difficult to interpret. [Michelet et al., 2012] have shown the latencies in experiment on the domestic cat, *Felis silvestris*.

The LSO and MSO extract location information with the use of different physical cues. The sensitivity of the system in dependence on the main sound frequency to sounds of different frequencies should be different.

In the extant human, the MSO is the larger of the two nuclei and contains approximately 10000 - 11000 neurons and the human LSO contains 5600 neurons [Moore, 2000]. As the loudness change discrimination implementation is much simpler that implementation of microsecond time delay in sound generation and processing, most of current auditory technology works as if the more important of the two nuclei were the LSO in *Homo sapiens*.

We have previously studied parameter free models of human sound localization. Current development of binaural cochlear implant technology enables to stimulate auditory periphery with rich repertoire of patterns. Better understanding to the MSO mechanisms will help to improve electrical hearing.

The range of sound frequencies processed in the MSO circuit is limited to the low frequency band. In human, where audible sound frequencies range from 20 Hz to 20 kHz, this low frequency band spans from 20 Hz to 1.5 kHz. Moreover, in the marginal values of this interval, performance of sound azimuth discrimination is worse. It is generally agreed that the main reason, why the workings of the MSO circuit deteriorate towards higher frequency is lowering of the synchronization of spike trains in the circuit with the sound source phase. The synchronization between two corresponding series of point events can be expressed as a discrete formula of vector strength, defined below in equation (1).

2 Methods

2.1 Preliminaries

Our procedures are mostly in using computational models, experimental data and statistical methods. Here we list several assumptions used in the paper. In any model of ITD based azimuth discrimination, time differences have to be computed with high accuracy in the range of tens of microseconds.

(1) For single MSO neuron model physical constants, especially time constants see [Toth and Marsalek, 2015]. In the single point neural model, membrane time constants are comparable to, or lower than 1 ms. These time constants govern neural spikes. They can capture time events in the range of microseconds or even tens of nanoseconds, as it has been shown elsewhere. (2) For the synaptic machinery, see [Toth and Marsalek, 2015] as well. (3) For the ergodic assumption see [Sanda and Marsalek, 2012], [Toth et al., 2018]. The basic set of parameters is shown in Table 1.

2.2 Model of the MSO neural circuit

Our model MSO circuit is based on connected phenomenological neurons. Input sound to left and right sides is transformed by the auditory periphery module into spike trains. Spikes in these trains are point events, only spike times matter and the details of spike numerical implementation do not make any differences in model output. These spike trains converge and diverge into higher order neurons. They are relayed from the auditory nerve and cochlear nucleus through the medial and lateral nuclei of trapezoid body up to the neurons of medial superior olive, which are first binaural neurons. Output of these neurons is the azimuth signal encoded in a spike train.

2.3 ITD readout curve

Let us have a monotonous function with firing rate as an input, which outputs azimuth. We will call it the ITD readout curve. In the paper by [Sanda and Marsalek, 2012] this curve is constructed by curve fitting to simulated points. Here we construct the curve based on assumption that the main frequency of sound input exist, is unique and is known. In addition to this known frequency, other parameters of the readout curve are set to make the fitting well posed and to obtain correct position of the curve maximum.

2.4 Vector strength

The vector strength definition is as follows, as it is used for example by [Goldberg and Brown, 1969]. Let us have sample spike phases φ_i, $i = 1, 2, \ldots, N$ relative to phases of a given input master periodic function, which does not enter the formula. The periodicity of tones making up speech is a perfect example of such stimulus. Discrete sum vector strength of sample $\varphi_1, \ldots, \varphi_N$ is defined as

$$R_{\mathrm{VS}}(\varphi_i) = \frac{1}{N}\sqrt{\left(\sum_{i=1}^{N}\cos\varphi_i\right)^2 + \left(\sum_{i=1}^{N}\sin\varphi_i\right)^2}. \tag{1}$$

2.5 JND and ideal observer

A higher variability of firing leads to a lower precision of the rate code. Intuitively, if a repeated presentation of the same stimulus evokes each time different spike count, then to distinguish between two different stimuli, the associated spike count change must be larger than the spike count variability. This way we determine the Just Noticeable Difference, JND of the rate code. In other words, this is the precision of rate coding.

We will ask whether it is possible to distinguish between two random processes with rates l_1 and l_2, $l_2 > l_1$. If we count events in a given counting window, we get counts n_1 and n_2. The probability that the observer obtains a result that $l_2 > l_1$ equals to the probability that $n_2 > n_1$. Let us assume that the random variables n_i, $i = 1, 2, \ldots$, have probability distributions $p(n_i)$ with means μ_i and equal standard deviation σ. A detection distance is then defined [Tanner Jr., 1961] as

$$d' = \frac{\mu_2 - \mu_1}{\sigma}. \tag{2}$$

This definition expresses the fact that the larger is the variance of the spike count, the worse is the detection capability. In psychophysics, a threshold value is commonly defined as that value for which the percentage of correct answers equals 75%. In our case, the examined value is the just-noticeable change of firing rate, $\Delta l = l_2 - l_1$. Assuming that both $p(n_1)$ and $p(n_2)$ are Normal (Gauss) distributed, the 75% probability of $n_2 - n_1 > 0$ corresponds to $d' = 1$. To obtain the JND of firing rate, we scale the detection distance with Δl and put $\delta' = d'/\Delta l$. Then, the JND of firing rate is

$$\Delta l_{\mathrm{JND}} = 1/\delta' = \frac{l_2 - l_1}{\mu_2 - \mu_1}\sigma. \tag{3}$$

3 Results

We investigate how circuit output and overall performance depend on sound frequency and sound intensity. All Figures show sample data of numerical simulation as black lines, lower estimate of data as blue lines and upper estimate of data as red lines.

Figure 1 shows how vector strength R_{VS} lowers towards higher frequencies, as it can be observed in the numerical module of the auditory periphery consisting of auditory nerve and cochlear nucleus. Vector strength cannot be larger than 1. The prevailing majority of neurons in the auditory pathway has vector strength spike train statistics sigmoidally dropping towards

higher sound frequencies as it is in this example. In this figure, data originally recorded by [Joris, 1996] at the MSO of domestic cat, were fitted to the sigmoidal curve with the general formula of the Boltzmann function used in [Marsalek and Lansky, 2005]. The curve fit of vector strength R_{VS} in dependence on sound frequency F_{S} is:

$$R_{\mathrm{VS}} = (1 + \exp(K_{\mathrm{S}} f_{\mathrm{S}} - K_{\mathrm{C}} F_{\mathrm{C1/2}}))^{-1}, \tag{4}$$

where K_{S}, sound coefficient; K_{C}, critical coefficient; and $F_{\mathrm{C1/2}}$, critical half frequency; are proportionality constants. Note that at sound frequencies from 20 to 100 Hz, there are two branches reflecting the existence of two alternative ways how to compute the lower limit, see Discussion section.

Figure 2 shows the curves limiting the ITD obtained with the basic parameter set in dependence on the sound frequency. The quadratic curve fit of the JND denoted Δt_{JND} is:

$$\Delta t_{\mathrm{JND}} = A(f_{\mathrm{S}} - F_{\mathrm{C1/2}})^2 + B, \tag{5}$$

where upper and lower bound parameters A and B are fitted constants and the other parameters and variables are as above. See also [Zwislocki and Feldman, 1956]. Analogously to Figure 1, sound frequencies from 20 to 100 Hz exhibit higher spread between lower and upper limits, as the fitting method (quadratic fit) is the same for both limits.

Figure 3 shows how the JND of ITD depends on timing jitter magnitude t_{J}. There are several time constants, which are defined in relation to physical properties of spatial sound processing. *Critical* timing jitter is lower estimate of timing jitter captured by spike train of typical mammalian neuron, $T_{\mathrm{JC}} = 0.2$ ms. *Normalized* value timing jitter $T_{\mathrm{JN}} = 1$ ms is the value of timing jitter normalized in relation to the output JND with respect to average firing rate. *Optimal* value timing jitter $T_{\mathrm{JO}} = 1.66$ ms is result of crossing two fits described below.

Simulations show that with lowering timing jitter the circuit output is virtually more and more precise. Yet, when the jitter is lower than critical value T_{JC}, determined by intrinsic noise, duration of coincidence detection window, and by other time constants, the precision lowers again. The two curves fitted to the simulation are:

1. fit of exponential function to simulations, red curve:

$$\Delta t_{\mathrm{JND}} = \exp(A_1(t_{\mathrm{J}} - B_1)) - C_1, \tag{6}$$

where $A_1 = 1.9$, $B_1 = 1.25$ and $C_1 = 0.2$ are fitted parameters. This relation is shown conveniently by the logarithmic y-axis in this figure.

2. Another fit, which also takes into account shot noise in lower jitter values, is to a quadratic function, blue curve:

$$\Delta t_{\mathrm{JND}} = A_2(t_{\mathrm{J}} - B_2)^2 + C_2, \tag{7}$$

where $A_2 = 2.5$, $B_2 = 1$, $C_2 = 1$. There is only one parameter sought by numerical simulation. This is A, fitted to data, as the point $(x, y) = (B_2, C_2)$ has been chosen to be a unit. This fit is the normalized fit of the model.

Logarithm of the simulated JND lowers with the exponential curve (6), which is concave function of sought jitter t_{J} as the jitter gets lower. The trend towards higher accuracy diverges from the parabolic fit in equation (7), when jitter reaches critical value between T_{JC} and T_{JO}.

$$T_{\mathrm{JC}} = 0.2 \lessapprox t_{\mathrm{J}} \lessapprox T_{\mathrm{JO}} \lessapprox 2\mathrm{ms}. \tag{8}$$

Beyond that point towards the lower jitter values, the neural circuit cannot function properly, as too low jitter prevents the interaction of spikes from the left and right side within the coincidence detection mechanism.

This corresponds to the analytical dependency obtained in [Salinas and Sejnowski, 2000] for a perfect integrator model with several inputs. The mechanism studied thereof is close to the MSO neural mechanism studied here. The firing rate changes in dependency on the input spike timing variability of *partially correlated* input spike trains.

Figure 4 shows the ITD readout curve. The rising slope of this curve is used as a readout function yielding the firing rate in dependency on the ITD, which in turn signals the sound azimuth to the next nuclei of the auditory pathway.

4 Discussion

In this paper we have revisited numerical simulations by [Sanda and Marsalek, 2012]. We have added analytical estimations to the description of the MSO function which have not been known previously. Our analytical calculations make possible to derive time constants useful in description and design of normal human hearing, hearing with hearing aids and cochlear implants. All Figures contain analytically expressed upper and lower limits in their transfer functions or other functional descriptions.

Figure 1 contains two lower limit branches at low frequencies. Limiting lower bound by two different analytical functions (branches) can be understood as uncertainty. A conservative estimate always considers the lower of the two branches. This uncertainty should be recognized as one of original results presented for the first time in this paper. Its existence has been proposed in a thesis by [Bures, 2014]. A comparison of model of low frequency stochastic computation in the MSO with psychoacoustical experiments is currently in preparation by [Bures and Marsalek, 2020].

Figure 2 depicts a quadratic fit. This fit is after linear regression the simplest analytical way, how to capture nonlinear and band limited span of human hearing range. Even simplest polynomial and nonlinear fits might exhibit nontrivial and not that simply tractable outputs, when subject to neuronal computation [Bures, 2014].

Figure 3 calculations use assumptions about intrinsic noise [Bures, 2014]. The simulation data have been obtained by arbitrary precision calculation. Any neural recording cannot reach this precision due to the internal noise of both neurons and recording electronic. In order to capture this property, we have used both exponential and quadratic fits. When we attempt to use them as upper and lower bounds, we notice that they exchange their order in region close to the optimal jitter value. In accordance with other Figures in this paper we use color coding for the upper and lower bound and different branches of the two fits are denoted by different data-points. In other words, at the lower jitter values the two estimates exchange their ordering. This is the choice of the quadratic fit to obtain a normalized bound together with other data-points. Numerical simulation with the basic set of parameters at $x = 1$ ms lies beyond this point, but close to the exponential fit.

Figure 4 contains better fit of the Sine function, as compared to [Sanda and Marsalek, 2012]. As lower bound we can also use circular Normal density function, the difference is negligible, not shown [Toth et al., 2018]. Comparison of time constants and sound periods in the model presented here will answer a tentative question: What is the highest slope of the ITD interpolation curve, such that it gives the resolution of 4°, angular degrees, in the ITD = 0 direction? This

slope is more steep in higher frequency sounds, its maximum is attained in maximum frequency of the MSO circuit operation, around 1 kHz [Marsalek and Lansky, 2005].

Towards the analytical descriptions it is important to note that other periodic functions can be used as the ITD readout curves. In [Toth et al., 2018] we have compared the Sine function with the circular Beta density, and other alternative functions. To impose periodic and infinite boundaries to the problem, regular Normal density and circular Normal density have been used and tested in previous versions of our model. No differences between these densities with proper parameters have been shown by common statistical tests when testing differences between two probability densities, ibidem.

[Franken et al., 2014] use recorded spike trains of several nuclei in the MSO neural circuit to demonstrate that coincidence detection is an essential part of the neuronal arithmetic [Bures, 2012] executed by the neural circuit. These are simulations combined with experimental description of MSO workings in line with our concepts and coincidence detection theories.

Another MSO model, already studied in 2005 is: [Zhou et al., 2005], this is a great example of simplistic model, motivating the description presented in this paper. For discussion of neural coding in the auditory nerve, cochlear implants and MSO see [Kerber and Seeber, 2012].

Our investigation of quantitative properties of the superior olive neural circuit is also motivated by the three LSO experimental papers, which have detailed methodology applicable to LSO, to the overlap of sound frequency ranges between the LSO and the MSO; and also to the MSO range itself; [Joris and Yin, 1995]; [Joris, 1996]; [Joris and Yin, 1998].

Following his notoriously known paper from 1948, Lloyd A. Jeffress dedicated lots of efforts to the search of a mechanism, by which microsecond time scale events of directional sound difference can be transformed into a code processed and transmitted by action potentials lasting several microseconds [Jeffress et al., 1962]. Historical comments on Jeffress papers are summarized by Cariani in Scholarpedia [Cariani, 2011]. A plausible explanation of the microsecond precision of the MSO circuit describes the neural computation by leading edges of action potentials and post-synaptic potentials, [Marsalek, 2000], [Toth et al., 2018].

Starting from: [Marsalek, 2000], authors of this paper investigated individual steps of signal processing in the superior olive neural circuits. Various synaptic mechanisms have been proposed [Marsalek and Kofranek, 2005]. Jitter and spike variability has been systematically analytically investigated by [Kostal and Marsalek, 2010].

In this last paragraph of Discussion section, we should mention briefly rest of scientific papers, where we found ides towards the design of the mechanistic model presented here. Article by [Michelet et al., 2012] discusses interaural phase delays (IPDs; when they exist, they are equivalent to the ITDs) and cochlear delays. For cochlear delays, very important is to review the ranges of delays in comparison to sound periods and classically described excitatory-excitatory and excitatory-inhibitory responses to binaural inputs in [Joris et al., 2006]. Paper of Srinivasan, Laback and Majdak cites current progress of ITD encoding by binaural cochlear implants, this is important for model validations and applications to studies with hearing aids and electrical hearing, [Srinivasan et al., 2018].

Conclusions

This theoretical paper is continuation of sound localization precision descriptions in the MSO [Sanda and Marsalek, 2012] and in the LSO [Bures and Marsalek, 2013]. Novel results are two: 1) analytical estimates of results obtained previously only by numerical simulation and 2)

comparison of natural and electrical hearing modalities and demonstrating what is the maximum timing precision which can be attained by the two modalities.

Acknowledgments

This project was in part funded by Charles University graduate students research program, acronym SVV, No. 260371/ 2016-2019, to Petr Marsalek and Marek Hajny. We acknowledge uploading this manuscript first to ArXiv repository prior to impacted journal submission. Special thanks to Pavel Sanda for permission to use his simulations and to Marek Hajny for reading and commenting the manuscript.

Author contributions

Model design: PM, ZB. Methodology: PM, TBA. Writing original draft: PM. Writing editing: ZB, PM, TBA.

Technical, TEX Typesetting, Archiving Notes

Compilation notes: LATEX compilation date is November 23, 2019.
BibTEX output: circa 30 is estimated references count (as of November 20, 2019).
Version of sources in octave is 2019.1.3, version of manuscript is 2019.A.1.
Complete sources web link under password: `http://nemo.lf1.cuni.cz/mlab/ftp/ftp/bures-z`
Preview web link: `http://nemo.lf1.cuni.cz/mlab/ftp/ftp/to-be-added`
Things to do to by co-authors:
Petr Marsalek. Clean up and finish first pass writing.
(Third) To Be Author is kindly asked to help the author team with tasks: 1) reading Discussion
2) checking up figures.
Zbynek Bures. Should do internal English language copy-editing. final reading of the manuscript before submission to the journal.

References

[Bures, 2012] Bures, Z. (2012). The stochastic properties of input spike trains control neuronal arithmetic. *Biol. Cybern.*, 106(2):111–122.

[Bures, 2014] Bures, Z. (2014). Internal representation and processing of acoustic stimuli in the nervous system. Habilitation thesis. *VUTIUM, Brno, Czech Republic*, pages 1–122.

[Bures and Marsalek, 2013] Bures, Z. and Marsalek, P. (2013). On the precision of neural computation with the interaural level difference in the lateral superior olive. *Brain Res.*, 1536:111–122.

[Bures and Marsalek, 2020] Bures, Z. and Marsalek, P. (2020). Discrimination of sound intensity at low frequencies: models and psychophysics. *ArXiv In Preparation*, N/A:N/A.

[Cariani, 2011] Cariani, P. (2011). Jeffress model. *Scholarpedia*, 6(7):2920.

[Franken et al., 2014] Franken, T. P., Bremen, P., and Joris, P. X. (2014). Coincidence detection in the medial superior olive: mechanistic implications of an analysis of input spiking patterns. *Front. Neural Circuits*, 8(42):1–21.

[Goldberg and Brown, 1969] Goldberg, J. M. and Brown, P. B. (1969). Response of binaural neurons of dog superior olivary complex to dichotic tonal stimuli: some physiological mechanisms of sound localization. *J. Neurophysiol.*, 32(4):613–636.

[Grothe et al., 2010] Grothe, B., Pecka, M., and McAlpine, D. (2010). Mechanisms of sound localization in mammals. *Physiol. Rev.*, 90(3):983–1012.

[Jeffress et al., 1962] Jeffress, L. A., Blodgett, H. C., and Deatherage, B. H. (1962). Effect of interaural correlation on the precision of centering a noise. *J. Acoust. Soc. Am.*, 34(8):1122–1123.

[Joris et al., 2006] Joris, P. X., Van de Sande, B., Louage, D. H., and van der Heijden, M. (2006). Binaural and cochlear disparities. *Proc. Natl. Acad. Sci. USA*, 103(34):12917–12922.

[Joris and Yin, 1995] Joris, P. X. and Yin, T. C. (1995). Envelope coding in the lateral superior olive. I. Sensitivity to interaural time differences. *J. Neurophysiol.*, 73(3):1043–1062.

[Joris, 1996] Joris, P. X. (1996). Envelope coding in the lateral superior olive. II. Characteristic delays and comparison with the responses in the medial superior olive. *J. Neurophysiol.*, 76(4):2137–2156.

[Joris and Yin, 1998] Joris, P. X. and Yin, T. C. (1998). Envelope coding in the lateral superior olive. III. Comparison with afferent pathways. *J. Neurophysiol.*, 79(1):253–69.

[Kerber and Seeber, 2012] Kerber, S. and Seeber, B. U. (2012). Sound localization in noise by normal-hearing listeners and cochlear implant users. *Ear Hear.*, 33(4):445–457.

[Kostal and Marsalek, 2010] Kostal, L. and Marsalek, P. (2010). Neuronal jitter: can we measure the spike timing dispersion differently? *Chinese J. Physiol.*, 53(6):454–464.

[Marsalek, 2000] Marsalek, P. (2000). Coincidence detection in the Hodgkin-Huxley equations. *Biosystems*, 58(1-3):83–91.

[Marsalek and Kofranek, 2005] Marsalek, P. and Kofranek, J. (2005). Spike encoding mechanisms in the sound localization pathway. *Biosystems*, 79(1-3):191–8.

[Marsalek and Lansky, 2005] Marsalek, P. and Lansky, P. (2005). Proposed mechanisms for coincidence detection in the auditory brainstem. *Biol. Cybern.*, 92(6):445–451.

[Michelet et al., 2012] Michelet, P., Kovacic, D., and Joris, P. X. (2012). Ongoing temporal coding of a stochastic stimulus as a function of intensity: time-intensity trading. *J. Neurosci.*, 32(28):9517–9527.

[Mills, 1958] Mills, A. W. (1958). On the minimum audible angle. *J. Acoust. Soc. Am.*, 30(4):237–246.

[Moore, 2000] Moore, J. K. (2000). Organization of the human superior olivary complex. *Microsc. Res. Tech.*, 51(4):403–412.

[Salinas and Sejnowski, 2000] Salinas, E. and Sejnowski, T. J. (2000). Impact of correlated synaptic input on output firing rate and variability in simple neuronal models. *J. Neurosci.*, 20(16):6193–6209.

[Sanda and Marsalek, 2012] Sanda, P. and Marsalek, P. (2012). Stochastic interpolation model of the medial superior olive neural circuit. *Brain Res.*, 1434:257–265.

[Simmons et al., 1998] Simmons, J. A., Ferragamo, M. J., and Moss, C. F. (1998). Echo-delay resolution in sonar images of the big brown bat, *Eptesicus fuscus*. *Proc. Natl. Acad. Sci. USA*, 95(21):12647–12652.

[Srinivasan et al., 2018] Srinivasan, S., Laback, B., Majdak, P., and Delgutte, B. (2018). Introducing short interpulse intervals in high-rate pulse trains enhances binaural timing sensitivity in electric hearing. *J. Assoc. Res. Otolaryngol.*, 19(3):301–315.

[Tanner Jr., 1961] Tanner Jr., W. P. (1961). Physiological implications of psychophysical data. *Ann. N. Y. Acad. Sci.*, 89(5):752–765.

[Toth and Marsalek, 2015] Toth, P. G. and Marsalek, P. (2015). Analytical description of coincidence detection synaptic mechanisms in the auditory pathway. *Biosystems*, 136:90–98.

[Toth et al., 2018] Toth, P. G., Marsalek, P., and Pokora, O. (2018). Ergodicity and parameter estimates in auditory neural circuits. *Biol. Cybern.*, 112(1-2):41–55.

[Zhou et al., 2005] Zhou, Y., Carney, L. H., and Colburn, H. S. (2005). A model for interaural time difference sensitivity in the medial superior olive: interaction of excitatory and inhibitory synaptic inputs, channel dynamics, and cellular morphology. *J. Neurosci.*, 25(12):3046–3058.

[Zwislocki and Feldman, 1956] Zwislocki, J. and Feldman, R. (1956). Just noticeable differences in dichotic phase. *J. Acoust. Soc. Am.*, 28(5):860–864.

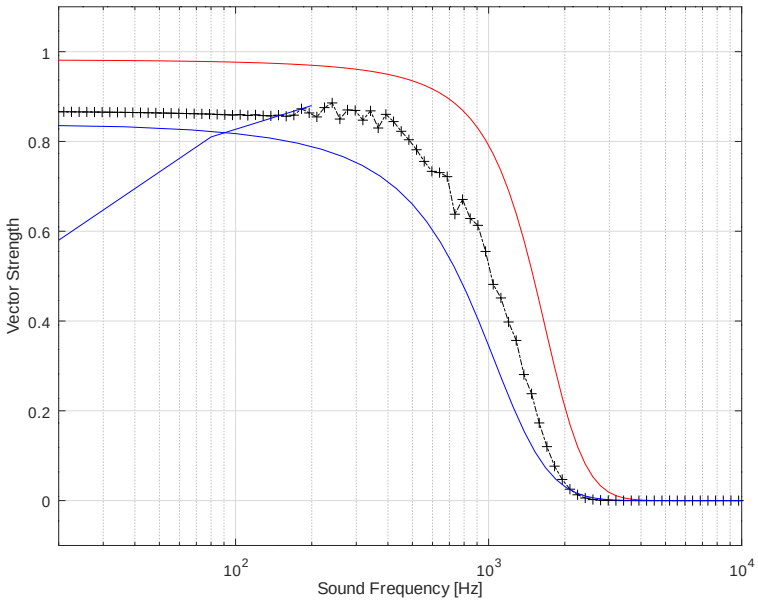

Figure 1: **Vector strength of auditory nerve spike trains in dependence on sound frequency.** X-axis shows sound frequency in Hz in logarithmic scale and y-axis shows the vector strength. Even though in some nuclei up the auditory pathway the synchronization can be maintained towards higher frequencies than shown here, the decrease of the vector strength towards higher frequencies is a general property of all neurons in the auditory pathway. Red curve shows upper theoretical limit and blue curve shows lower limit. Black points are data simulated with the use of point-process-spikes train generation with the use of the dead time Poisson process. Note that in frequency f_{S} range from 20 to 100 Hz the lower limit is shown by two curves, the upper is the Boltzmann function fit and the lower is decrease of vector strength at low frequencies due to stochastic response of high spontaneous rate neurons.

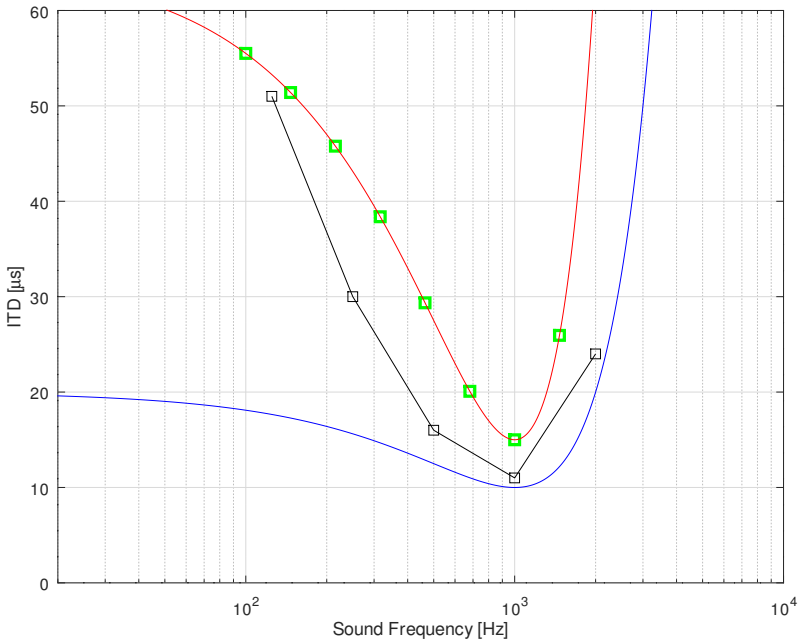

Figure 2: **The shortest JND of ITD detected in the dependence on sound frequency.** X-axis shows sound frequency in Hz in a logarithmic scale and y-axis the shortest JND of ITD in μs. This is a theoretical prediction based on the analytical model and basic parameter set used in simulations. As in other figures, black line is obtained by simulation and red and blue lines are respectively upper and lower bounds obtained by an analytic fit.

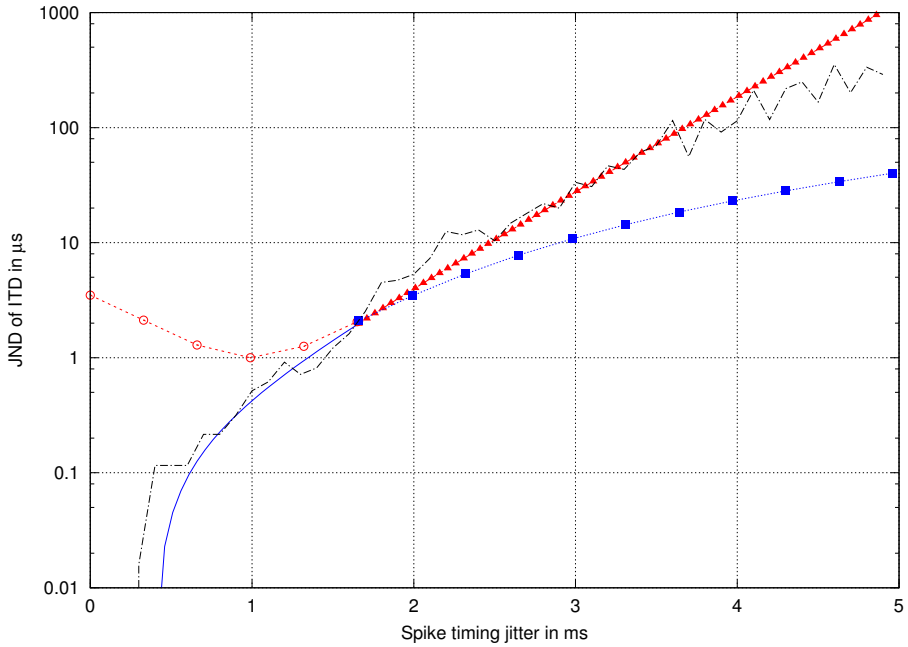

Figure 3: **Just noticeable difference values in basic parameter set in dependence on the jitter magnitude.** This plot in semi-logarithmic y-scale shows JND (just noticeable difference) of interaural time difference depending on variation of the spike timing jitter. Jagged black line: simulated data, solid line: an exponential fit to the simulations under the assumption of arbitrary time precision in the model circuit, dotted line: a quadratic function estimate of spike timing precision in a system with addition of noise. Note that in this figure the exponential and quadratic fits cross at $f_{\mathrm{S}} = 1.66$ ms. In order to correspond to other figures showing the upper and lower bounds of the estimate of stochastic model, the two fits are split into two branches of the same function at this point of $f_{\mathrm{S}} = 1.66$ ms. For lower x values, quadratic fit is larger than the exponential, and vice versa. This is indicated by distinctive data-points. (These are circles and triangles; no data-points and squares, respectively.) Also notice that the curve of the quadratic fit goes through the point [1,1], this is a consequence of using normalized parameter set.

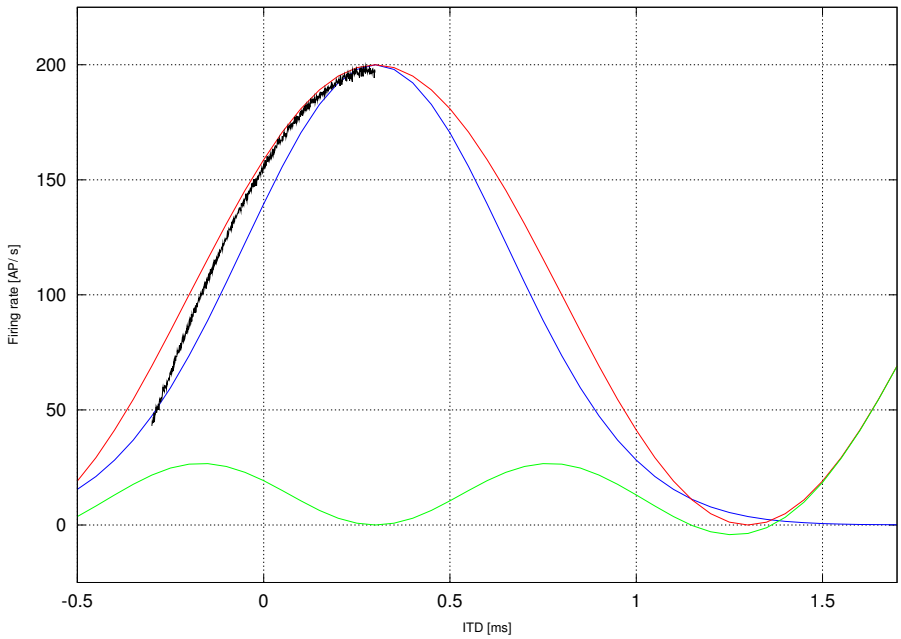

Figure 4: **Fit of example functions to firing rate slope ITD readout curve.** X-axis shows ITD in ms and y-axis shows corresponding firing rate in action potentials per second. Note that the curve peak is offset from the origin of coordinates at $t_{\mathrm{ITD}} = 0$. Red curve is sine function fit and blue curve is fit by the Normal density function with the variance set to correspond to the known sound main period. Green curve shows the difference between the red and blue curves.

Parameter	Symbol	Units	Typical Value	Ranges
Timing Jitter	t_{J}, σ	ms	1	0.125 - 8
Window of Coincidence Detection	w_{CD}	ms	0.6	0.15 - 1.5
Sound Frequency	f	Hz	200	40-1600
Shortest Perceptual Time	T_{PT}	ms	20	20 - 80

Table 1: The basic set of parameters.